10.1109/TIE.2015.2420617

Optimizing Photovoltaic Model for Different Cell Technologies Using A Generalized Multi-dimension Diode Model

Jing Jun Soon, *Student Member, IEEE* and Kay-Soon Low *Senior Member, IEEE*

Abstract—**Commercial photovoltaic (PV) modules are made of different PV cell technologies such as mono-crystalline, multi-crystalline, amorphous silicon and copper indium diselenide (CIS). Usually, a single or double diode PV model is used to model the output characteristic. However, it is unclear that which PV model is optimal for each PV cell technology as the modeling accuracy is dependent on the PV model used. To fill up this research gap, a generalized multi-dimension (*n* by *m*) diode PV model is proposed in this paper to determine the optimal PV model. The proposed PV model allows the diode network to be configured to better fit the output characteristics of different PV cell technologies. Both simulation and experimental results are presented to illustrate the advantages of the proposed model. From the results, the optimal PV model that matches each of the cell technology is established. They can be used as reference PV model for future works.**

Index Terms— **Double diode PV model, multi-diode PV model, optimal PV model, particle swarm optimization (PSO), PV cell technologies, PV modeling, single diode model.**

I. INTRODUCTION

IN a photovoltaic (PV) power system, the PV model is used to study the amount of energy that is available for the installation and also for maximum power point tracker simulation under different environmental conditions [1-6]. The simulation study is conducted before the actual implementation to ensure that the selected PV modules meet the system requirements.

A PV module output characteristic can be modelled by an electrical circuit. The commonly used models are the single and double diode PV models.

The single diode PV model (SDM) as shown in Fig. 1 (*n* = 1) has been widely used due to its fairly accurate result and low computational cost [7-12]. By identifying the five unknown parameters namely the photovoltaic current I_{pv}, diode saturation current I_0, ideality factor *a*, series resistance R_S and parallel resistance R_P, the output current-voltage characteristic can be modelled. However, its accuracy at the

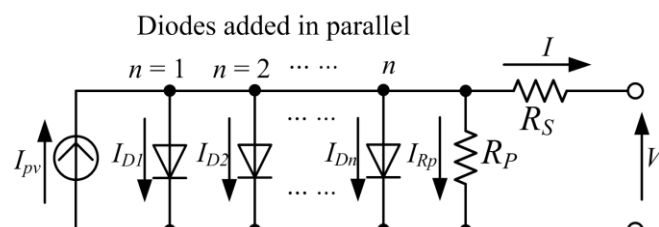open circuit voltage is inferior at low irradiance as the recombination loss is ignored [13-15].

Fig. 1 Electrical PV model: single diode PV model (*n* = 1), double diode PV model (*n* = 2) and three diode PV model (*n* = 3).

The modeling accuracy is improved using the double diode PV model (DDM) (*n* = 2) by introducing another diode in parallel to the SDM. This is to account for the recombination losses resulting in more accurate cell behavior at low irradiance [14, 16]. The DDM model has the same unknown parameters as the SDM with additional diode saturation current and ideality factor for the second diode.

Further improvement can be made to the DDM by introducing a third diode known as the three diode PV model (*n* = 3) [17] (TDM). This is to correctly model the effects of grain boundaries and leakage current due to periphery.

Although DDM and TDM are able to describe the physical underlying in the PV modules, they are also more computational expensive due to the extra diodes [18]. From these studies, it is observed that there is a trend of increasing the number of diodes of the PV model in parallel to achieve a more accurate result. However, the accuracy of the SDM, DDM and TDM to model the physical underlying effects remains unknown [16, 19].

Using the SDM or DDM, the output characteristic of different PV cell technologies namely mono-crystalline, multi-crystalline, amorphous silicon and copper indium diselenide (CIS) have been modelled in previous works [8, 14, 20-27]. The results show that the modeling accuracy is dependent on the PV model used to represent the type of cell technology [25, 26].

To better represent the output characteristic of a particular cell technology, adding a sink current source to the SDM to describe the recombination current in the intrinsic layers of the amorphous silicon PV cell technology [19, 28] has been presented. As crystalline cell technology do not have intrinsic layer, this modification is only suitable for amorphous PV cell technology.

In this paper, a generalized multi-dimension diode PV model as shown in Fig. 2 is proposed. When compared with existing PV models that only increase the number of diodes in parallel to increase the accuracy, the <mark>proposed</mark>

J. J. Soon is with Satellite Research Centre (SaRC), School of Electrical and Electronic Engineering, Nanyang Technological University, 50 Nanyang Avenue, Singapore 639798. Phone: +65 6790 6522; e-mail: jjsoon@ntu.edu.sg.

K. S. Low is with is with Satellite Research Centre (SaRC), School of Electrical and Electronic Engineering, Nanyang Technological University, 50 Nanyang Avenue, Singapore 639798. E-mail: k.s.low@ieee.org.

multi-dimension PV model allows the diodes to be placed in series and parallel. This provides a configurable diode network to better suit the different PV output characteristic.

The unknown parameters of the proposed PV model are identified using an improved version of particle swarm optimization (PSO) method presented in [25]. As compared to the PSO method in [25], the improved PSO uses two additional data points namely the short circuit current and open circuit voltage to determine the best set of parameters.

The improved PSO method is validated by comparing with two popular methods [8] and [14] used to determine the unknown parameters for the SDM and DDM. The results indicate that the proposed method has better accuracy under different operating temperature.

The fundamental idea of using multi-dimension diode for the modeling of PV modules was first reported in [29]. However, the underlying principle on how the diodes should be configured to best model different PV cell technologies has not been addressed. In this paper, it is shown that the adding of diodes in series would lead to larger *I-V* curve coverage as compared to the SDM and DDM. To reduce the higher computational cost of [29], this paper redefines the diode saturation of the multi-dimension diode PV model to reduce the number of unknowns by *n*. In addition, 13 PV modules of different cell technologies have been investigated and their optimal models have been determined.

This paper is organized as follows: Section II provides an overview of the PV mathematical model. Section III investiages the *I-V* coverage of different PV models by varying their parameters. Section IV presents the proposed algorithm to identfy the unknown model parameters. Section V presents the modeling results used to determine the optimal PV model for each cell technology. Finally, Section VI summarizes the work.

II. MATHEMATICAL MODEL OF PV MODULE

The circuit model of the proposed multi-dimension diode PV model is shown in Fig. 2. It has *m* diodes connected in series and *n* strings of diodes in parallel. It's operating conditions at short circuit, open circuit and maximum power point have been presented in [29].
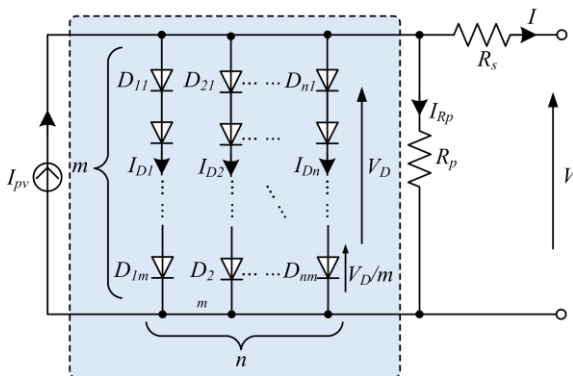

Fig. 2 Proposed generalized multi-dimension diode PV model.

Under different operating light intensity and temperature, the PV output is affected. The relationship of photovoltaic current due to light intensity *G* and operating temperature *T* can be found in [30, 31]. Likewise, the relationship of short circuit current, open circuit voltage, maximum power current,

maximum power voltage due to temperature have been studied in [29].

It should be noted that the maximum power temperature coefficient is not a constant [32]. To account for this variation, the maximum power voltage V_{mp} and current I_{mp} at *T* is multiplied to obtain the temperature dependent $P_{mp}(T)$.

Given the photovoltaic current, the remaining unknowns for the generalized multi-dimension diode model are the diode saturation currents, ideality factors, series and parallel resistances.

For SDM and DDM, the diode saturation current is a function of ideality factor and it can be reduced. The reduced model has similar accuracy and has been previously validated in [8, 14].

In this work, a similar reduced model is used for the multi-dimension diode PV model. The resultant diode saturation current of nth diode string with respect to temperature is expressed as

$$I_{0,n}(T) = \frac{I_{SC}(T)}{\left[\exp\left(V_{OC}(T)m \Big/ N_S V_t \sum_{i=1}^{m} a_{ni} \right) - 1 \right]} \quad m > 1$$

(1)

where the terms $I_{SC}(T)$, $V_{OC}(T)$ and *a* are the short circuit current, open circuit voltage and ideality factor at temperature *T* respectively.

When *m* = 1, the diode saturation current can be simplified as in [8]. For the case that *m* > 1, the diode saturation current in the proposed multi-dimension diode model becomes another parameter that changes the model's output characteristic.

From (1), it is observed that the ideality factor in the diode saturation current is taken to be the average value of ideality factors of the particular string. This is to reduce the computation cost as compare to the work in [29] where the ideality factor of the diode saturation is taken to be another unknown. For 100 sets of unknown parameters, the optimization process for *n1m3* (*n* = 1, *m* = 3) PV model using MatLab running on Intel i7 3.4GHz PC is reduced from 7.98 seconds to 3.53 seconds.

III. *I-V* AND *P-V* CURVES COVERAGE

The shapes of the *I-V* and *P-V* curves depend on the values of the ideality factor, series and parallel resistances. The way the *I-V* and *P-V* curves change by varying ideality factor, series and parallel resistances have been studied in [24, 33]. However, the effect of additional diodes in series on the PV characteristic curves has not been addressed.

In the following study, the ideality factor of the SDM is varied from 0.5 to 2 with a step of 0.01, series resistance from 0 to 1 and parallel resistance from 10 to 100.

A. *Effects of series and parallel resistance on SDM*

The effects of the series and parallel resistance on SDM (*n* = *m* = 1) are investigated in this section. The corresponding *I-V* and *P-V* curves are shown in Figs. 3 and 4 respectively.

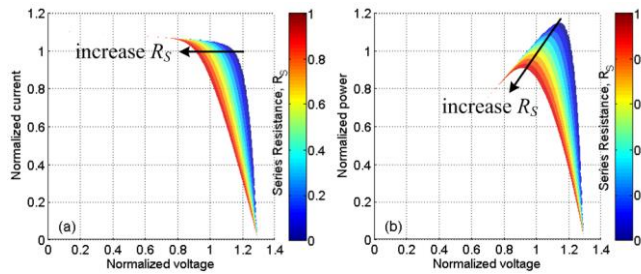Fig. 3 Effect of series resistance on single diode PV model, (a) *I-V* curves and (b) *P-V* curves under 1000 W/m^2, 25 ^{o}C and A.M 1.5.
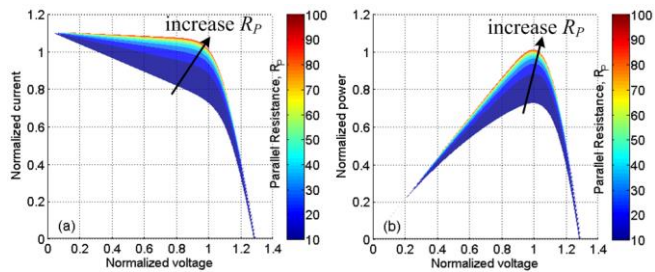

Fig. 4 Effect of parallel resistance on single diode PV model, (a) *I-V* curves and (b) *P-V* curves under 1000 W/m^2, 25 ^{o}C and A.M 1.5.

In Figs. 3 and 4, the *x* and *y* axes are normalized to the maximum power point (MPP), maximum power voltage and current. Hence, the coordinates $x = y = 1$ represent the MPP.

From Fig. 3(a), the increase in series resistance shifts the *I-V* curves to the left and lowers the peak of the *P-V* curves in Fig. 3(b). In addition, the gradient of the slope after the MPP become less steep with the increase in series resistance.

On the other hand, an increase in the parallel resistance shifts the *I-V* and *P-V* curves to have a higher MPP as shown in Fig. 4. Moreover, the effects of the parallel resistance become insignificant when it becomes large.

Using these two parameters, the shape of the slope before and after the MPP can be tuned to match the *I-V* and *P-V* curves of the PV module. If the *I-V* or *P-V* curves to be modelled are not within the coverage region of the PV model, the ideality factor can be used as another degree of freedom to adjust the *I-V* and *P-V* curves as discussed in the next section.

B. Effects of ideality factor on SDM (n = m = 1)

For a mono-crystalline PV module, the ideality factor range from 1 to 2 [34]. The relationship between the *I-V* and *P-V* curves with different ideality factors are illustrated in Fig. 5.
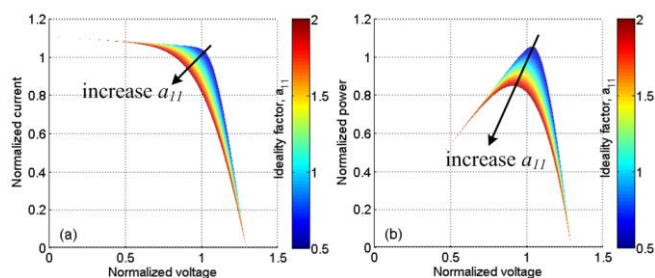

Fig. 5 Coverage of single diode PV model by varying the ideality factor a_{11}, (a) *I-V* curves and (b) *P-V* curves under 1000 W/m^2, 25°C and A.M 1.5.

Unlike the effect of series and parallel resistance, the ideality factor does not affect the *I-V* and *P-V* curves before or after the MPP as shown in Fig. 5. Instead, an increase in the ideality factor causes the area around the MPP to have a wider

span. The amount of span at the MPP can be increased by adding another diode in parallel, realizing the DDM.

C. Double diode PV model (n = 2, m = 1)

Fig. 6 shows the *I-V* and *P-V* curves of the double diode PV model by varying a_{11} and a_{21}.
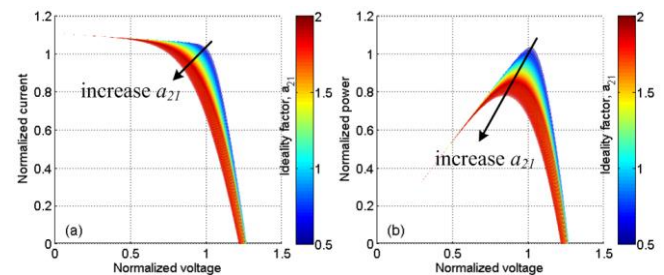

Fig. 6 Coverage of double diode PV model by varying the ideality factor a_{11} and a_{21}, (a) *I-V* curves and (b) *P-V* curves under 1000 W/m^2, 25°C and A.M 1.5.

By comparing Fig. 6 to Fig. 5, the span at the MPP of the DDM is wider than SDM. The coverage area can be further extended by introducing addition diodes in series proposed in this paper.

D. n1m2 PV diode model (n = 1, m = 2)

For the n1m2 diode PV model, it is the SDM with another diode connected in series with the existing diode. The ideality factors that can be varied are a_{11} and a_{12}. By varying them from 0.5 to 2 in step of 0.1, a family of *I-V* and *P-V* curves is generated as shown in Fig. 7.
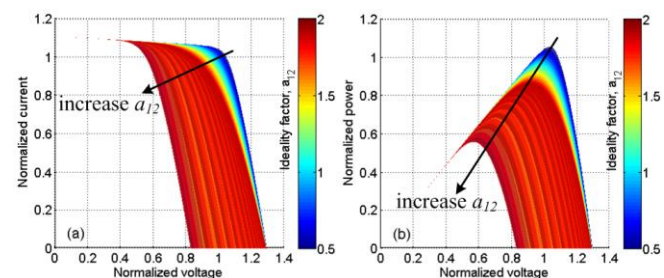

Fig. 7 Coverage of *n1m*2 diode PV model by varying ideality factors a_{11} and a_{12}, (a) *I-V* curves and (b) *P-V* curves under 1000 W/m^2, 25°C and A.M 1.5.

From Fig. 7, the coverage region of the *n1m*2 diode model is much larger as compared to the SDM and DDM. Additionally, the span at the MPP becomes much wider when a_{12} is increased from 0.5 to 2.

To further increase the coverage region, several diodes can be placed in series to form a string that can be connected in parallel. By doing so, we obtain the proposed generalized multi-dimension diode PV model.

IV. PARAMETERS IDENTIFICATION USING IMPROVED PARTICLE SWARM OPTIMIZATION WITH INVERSE BARRIER

There are two general approaches for identifying the unknown parameters of a PV model. The first approach uses the actual measurement such as the illuminated *I-V* [35, 36] or dark *I-V* curves [37]. By employing curve fitting or extrapolation methods, the unknown parameters of the PV model can be extracted.

The second approach uses equations derived from PV models and information readily available from the datasheet to extract the parameters. The unknown parameters are

obtained using explicit formulation [38, 39], iterations [8, 14] or optimization methods [20, 25]. In this approach, three data points namely the open circuit voltage, short circuit current and MPP are used.

In this paper, an improved version of the Particle Swarm Optimization (PSO) method in [25] is used to identify the unknown parameters of the multi-dimension diode PV model. This method belongs to the second approach that extracts the parameters based on information from the datasheet. As the PV output characteristic equation is transcendental, this method is selected to avoid partial differentiation and matrix inversion that may cause singularity.

The modified algorithm is presented in the following sections.

A. Relationship between number of diodes and unknown parameters

For the multi-dimension diode PV model, the unknown parameters to be identified are a_{ij}, R_S and R_P where $i = 1, 2 \ldots n$ and $j = 1, 2 \ldots m$. Therefore, the number of unknowns for the proposed model is given by

$$\begin{cases} 2+n & \text{for } m=1 \\ 2+(n\times m) & \text{for } m>1 \end{cases} \quad (2)$$

In (2), it is observed that when multiple diodes are connected in series ($m > 1$), the number of unknown parameters is increased by $n(m-1)$.

B. Generalized objective and inverse barrier function

Based on the three data points that are available from the manufacturer's datasheet, the objective function that is used to determine the unknown parameters is formulated. Using the PV modeling equations from [29], the objective function is expressed as

$$\min_{a_{ij},R_S,R_P,T} f_{obj} = \left| f_{I_{SC}} + f_{V_{oc}} + f_{P_{mp}} + f_{barrier} \right| \quad (3)$$

where

$$f_{I_{SC}}\left(a_{ij},R_S,R_p,T\right) = \frac{I_{SC}\left(I_{SC,e}(T),T\right)}{I_{SC,e}(T)}-1$$

$$f_{V_{OC}}\left(a_{ij},R_S,R_p,T\right) = \frac{V_{OC}\left(V_{OC,e}(T),T\right)}{V_{OC,e}(T)}-1 \quad \begin{array}{c} i=1,2...n \\ j=1,2...m \end{array} \quad (4)$$

$$f_{P_{mp}}\left(a_{ij},R_S,R_p,T\right) = \frac{P_{mp}\left(P_{mp,e}(T),T\right)}{P_{mp,e}(T)}-1$$

$$f_{barrier} = \mu \left[\sum_{i=1}^{n}\sum_{j=1}^{m}\beta_{aij}\left(\frac{1}{a_{ij,\max}-a_p}+\frac{1}{a_p-a_{ij,\min}}\right)\right.$$
$$+\beta_{Rs}\left(\frac{1}{R_{S,\max}-R_{S,p}}+\frac{1}{R_{S,p}-R_{S,\min}}\right)$$
$$\left.+\beta_{Rp}\left(\frac{1}{R_{P,\max}-R_{P,p}}+\frac{1}{R_{P,p}-R_{P,\min}}\right)\right] \quad (5)$$

The inverse barrier in (5) is added into the objective function to ensure that the resultant parameters are always positive.

TABLE I shows the constraint parameters for each PV cell technology used for optimization. The values are selected based on reported works in [34, 35, 40-42]. As the constraint values are different, a weightage $\beta_x = (x_{\max} - x_{\min})/4$ where $x = a_{ij}$, R_S or R_P are added to normalize the barrier function to unity. The subscript 'p' in (5) represents the present particle being evaluated and μ is the overall weightage for the barrier function.

It should be noted that the temperature T is formulated as a variable in (3)-(5). Thus the PV parameters are calculated for each temperature.

TABLE I
CONSTRAINT PARAMETERS FOR INVERSE BARRIER

	Mono-si	Multi-si	A-si	CIS	MJ-GaAs
$a_{ij\min}$	0.5	0.5	0.5	0.5	0.5
$a_{ij\max}$	2.0	2.0	5.0	2.0	5.0
$R_{S\min}$	0.001	0.001	0.001	0.001	0.001
$R_{S\max}$	1.000	1.000	3.000	3.000	3.000
$R_{P\min}$	50	50	50	50	50
$R_{P\max}$	1000	1500	1000	1000	5000

*Mono-Si, multi-Si, a-si, CIS, and MJ-GaAs represents mono-crystalline, multi-crystalline, amorphous silicon, copper indium diselenide and multi-junction gallium arsenic respectively.

C. The improved PSO algorithm

In [25], the optimal parameters are selected based on only the maximum power point given as $\left(\varepsilon_i = \left|P_{mp,i}(T)-P_{mp,e}(T)\right| + \left|V_{mp,i}(T)-V_{mp,e}(T)\right|\right)$ where ε is the overall model error and the subscript 'i' denotes the I-V curve being evaluated. This ensures that the I-V curve generated will have accurate MPP. Since only the MPP data point is used, the accuracy at the open circuit voltage and short circuit current may vary.

To have an accurate MPP, open circuit voltage and short circuit current, the proposed algorithm uses three data points to select the optimal parameters. The overall model error ε is redefine as

$$\begin{aligned} \varepsilon_i = &\left|P_{mp,i}(T)-P_{mp,e}(T)\right| \\ &+\left|V_{mp,i}(T)-V_{mp,e}(T)\right| \\ &+\left|I_{SC,i}-I_{SC,e}(T)\right|+\left|I_{Voc,i}(T)\right| \end{aligned} \quad (6)$$

where I_{voc} is the open circuit voltage current (ideally taken to be 0). Using (6), the I-V curve with the least model error is selected to be the best I-V curve.

The changes discussed in Section IV can be added into the pseudocode in [25] to realize the improved PSO algorithm.

V. RESULTS

For this study, the following parameters are selected:
1) population size N: 70;
2) maximum generation to be evaluated: 1000;
3) members of particle: a_{ij}, R_S and R_P where $i = 1, 2 .. n$ and $j = 1, 2 \ldots m$;
4) inertia weight factors: $\omega_{\max} = 0.9$ and $\omega_{\min} = 0.4$;
5) acceleration constants $c_1 = 2$ and $c_2 = 2$;
6) barrier parameter $\mu = 0.2$.

A. Validating the proposed identification method

The proposed parameter identification method in Section IV is validated by using three PV modules of different cell technologies [43-45].

The experimental data are obtained from the manufacturer's datasheets of the PV modules tested. They are extracted using GSview [46], which is a graphical tool that gives the pixel coordinates. Using the coordinates, the actual voltage and current values are then calculated. To ensure accurate *I-V* curves are extracted, the sample distance in the "knee" region of the *I-V* curves is kept at 1.5 pixels.

Using the proposed method, the unknown parameters are identified and they are used to plot out the *I-V* curves under different environmental conditions.

To benchmark the proposed method, the SDM [8] and the DDM [14] are compared with the proposed *n*1*m*1 and *n*2*m*1 PV model respectively. The ideality factor for the SDM and DDM are adjusted till the MPP is close to the manufacturer's MPP at STC for a fair comparison.

Fig. 8 shows the *I-V* curves of KD210GH-2PU PV module under different irradiances and temperatures. The red dash-dot line, blue solid line and green triangle markers are the SDM, *n*1*m*1 PV model and manufacturer's experimental data respectively. It is observed that the characteristic curves from the SDM and the proposed *n*1*m*1 model are close to the manufacturer's data despite changes in temperature and irradiance.
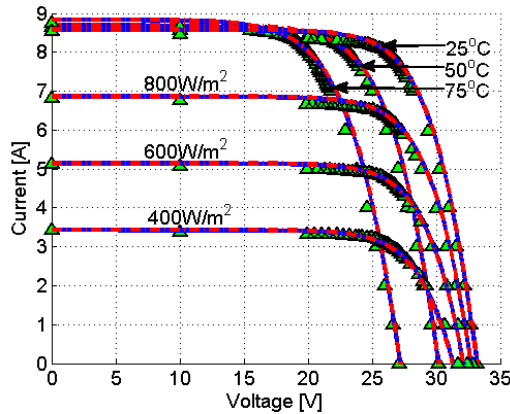

Fig. 8 *I-V* curves of single diode PV model [8] (red dash-dot line), proposed n1m1 PV model (blue solid line) and manufacturer's experimental data (green triangle marker) of KD210GH-2PU (multi-crystalline PV module) at different irradiances (*T* = 25 ºC) and temperatures (*G* = 1000 W/m^2).

To determine the accuracy of the model, the root mean square error (RMSE) is calculated. By denoting the manufacturer's experimental current as I and the PV model current as $\tilde{I}$, the normalized RMSE (NRMSE) is given as

$$NRMSE = \frac{1}{I_{mp,n}} \times \sqrt{\frac{1}{k} \sum_{j=1}^{k} \left(I_j - \tilde{I}_j \right)^2} \qquad (7)$$

where k represents the number of data points collected on each *I-V* curve.

Using (7), the NRMSE for the SDM, DDM, proposed *n*1*m*1 and proposed *n*2*m*1 PV models under different conditions are summarized in TABLE II.

Conditions		NRMSE (%)			
G (W/m^2)	T (ºC)	Single diode model [8]	n1m1 model	Double diode model [14]	n2m1 model
1000	25	1.850	1.707	9.018	4.829
1000	50	2.337	2.145	9.922	5.223
1000	75	2.750	2.404	9.116	4.622
800	25	1.492	1.455	7.144	2.351
600	25	1.522	1.380	5.815	2.236
400	25	1.760	1.528	3.928	2.810

From the results in TABLE II, the SDM and *n*1*m*1 PV model show similar accuracy while the *n*2*m*1 PV model achieved better accuracy than the DDM. The results also show that the *n*1*m*1 PV model is more accurate than the *n*2*m*1 PV model. This proves that the modeling accuracy varies with the use of different PV models.

To further validate the proposed model, the accuracy of the MPP is studied for ST-40 (CIS) and SP-70 (mono-crystalline) PV modules. Using the SDM, DDM, *n*1*m*1 and *n*2*m*1 PV models, the absolute P_{mp} and V_{mp} errors for ST-40 from -25 ºC to 75 ºC in step of 5 ºC are presented in Figs. 9 and 10 respectively. The presented results are based on an average of 20 datasets for each temperature.
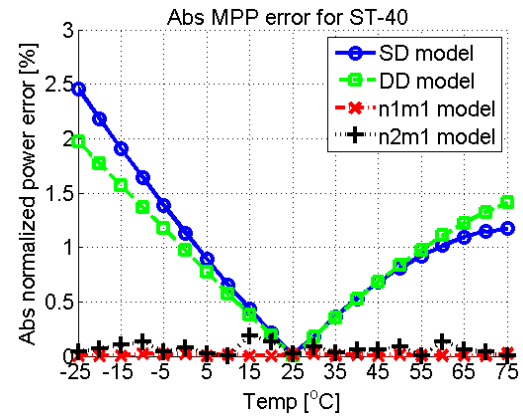

Fig. 9 Absolute MPP power error for ST-40 (CIS) at different temperature, *G* = 1000 W/m^2, A.M. = 1.5.
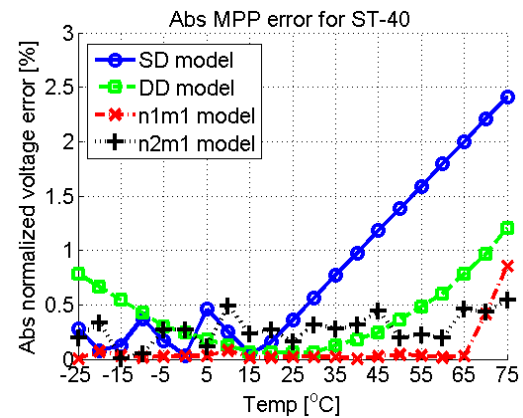

Fig. 10 Absolute MPP voltage error for ST-40 (CIS) at different temperature, *G* = 1000 W/m^2, A.M. = 1.5.

Based on the absolute MPP power error results in Fig. 9, it shows that the MPP power error using the SDM and DDM increases when the temperature is deviated away from 25 ºC. The maximum error of SDM and DDM are 2.46% and

1.973% respectively at T = -25 ºC. On the other hand, the absolute MPP power error of the proposed $n1m1$ and $n2m1$ PV model remains low throughout the temperature range. The absolute mean power error for SDM, DDM, $n1m1$ and $n2m1$ PV model are 0.992 %, 0.923 %, 0.011 % and 0.067 % respectively.

Similarly, the MPP voltage error with temperature varied from -25 ºC to 75 ºC for SDM, DDM, $n1m1$ and $n2m1$ PV models are shown in Fig. 10. The results show that if the temperature is greater than 15 ºC, the MPP voltage error of the SDM increases linearly to 2.41%. On the other hand, the MPP voltage error of the DDM increases as it deviates away from 25 º C. The maximum MPP voltage error occurs at T = 75 ºC is 1.205%.

For the proposed $n1m1$ PV model, it shows low MPP voltage error throughout the temperature range and a linear increase in error up to 0.855% after 65 ºC. Finally, the MPP voltage error of the proposed $n2m1$ PV model exhibit oscillation throughout the temperature range with a maximum error of 0.542% at T = 75 ºC. The absolute mean maximum power voltage error for SDM, DDM, $n1m1$ and $n2m1$ PV model are 0.820 %, 0.402 %, 0.086 % and 0.277 % respectively.

The absolute MPP power and voltage errors of SP-70 PV module are similar and the results are summarized in TABLE III.

In summary, the $n1m1$ and $n2m1$ PV models can achieve lower modeling error than SDM and DDM validating the proposed method. Moreover, using the same identification method for the $n1m1$ and $n2m1$ PV models, the modeling error is different proving that the modeling accuracy is dependent on the PV model used.

TABLE III
COMPARISON OF ABSOLUTE ERROR AT MPP FOR SINGLE DIODE, DOUBLE DIODE, PROPOSED N1M1 AND PROPOSED N2M1 PV MODEL FOR T = -25 ºC TO 75 ºC (G = 1000 W/M², A.M 1.5).

Method	Shell SP-70 (Mono-crystalline)			
	Mean (%)		Standard Deviation (%)	
	P_{mp} error	V_{mp} error	P_{mp} error	V_{mp} error
SDM [8]	1.279	0.231	0.764	0.230
DDM [14]	1.160	0.592	0.758	0.366
n1m1	0.005	0.036	0.003	0.025
n2m1	0.018	0.420	0.017	0.270

B. Selecting suitable PV model for each cell technology

In this section, thirteen PV modules [43-45, 47-56] of different PV cell technologies namely mono-crystalline, multi-crystalline, amorphous silicon, CIS and multi-junction gallium arsenic (MJ-GaAs) are used for the study. The number of diodes in the multi-dimension PV model are varied from n = m = 1 to 3 to change the output characteristic of the model. Then, the mean MPPE and mean NRMSE are studied to determine the optimal PV models for each PV cell technology.

A study on mono-crystalline PV cell technology is first conducted. The MPPE and NRMSE of different PV models for SP70, UPM250M and SM50 are presented in Fig. 11.

The absolute MPP error in terms of P_{mp} and V_{mp} errors are obtained by varying T = -25 ºC to 75 ºC in step of 5 ºC using the generalized multi-diode PV model. Each temperature is

repeated 20 times and the mean MPPE is taken for T = -25 ºC to 75 ºC represented by bar charts in Fig. 11.

From the 20 sets of parameters identified, they are used to generate I-V curves under different temperatures and irradiances. The mean NRMSE is then calculated represented by the dotted line with circle markers as shown in Fig. 11.

In Fig. 11, it is observed that the mean MPPE and the mean NRMSE are dependent on the choice of PV model. Moreover, the PV model that gives the lowest MPPE does not lead to the lowest NRMSE. With the increase of diodes in the PV model, the MPPE and NRMSE also increase. This is due to the increase in coverage region of the PV model resulting in more possibilities of generating an I-V curve that fulfill the cost function in (3).

The results in Fig. 11 also show that when n = 1 and m = 1 to 3, the mono-crystalline PV modules have lower MPPE and NRMSE as compared to other PV models.
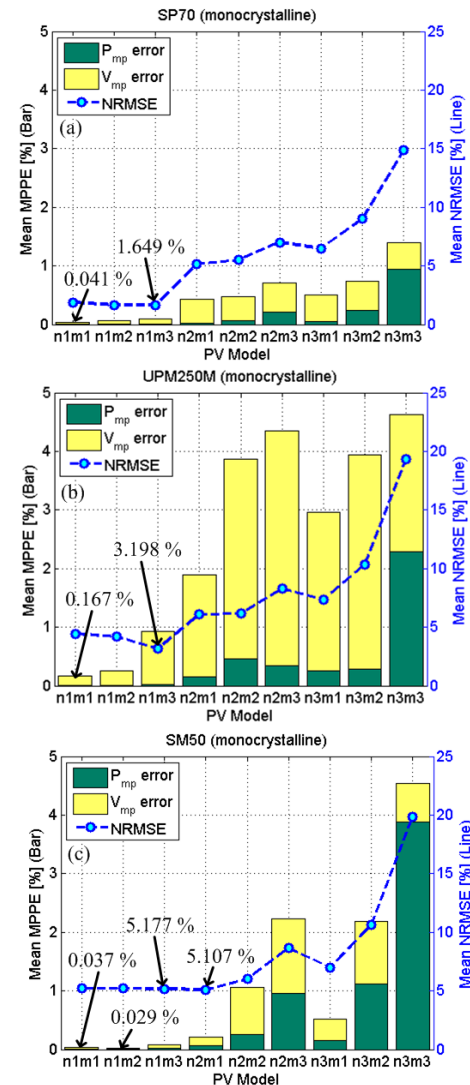
Fig. 11 Mean absolute maximum power point error over T = -25 ºC to 75 ºC and mean normalized root mean square error for mono-crystalline PV cell technology, (a) SP70, (b) UPM250M and (c) SM50.

From Figs. 11(a) and (b), the SP70 and UPM250M PV modules have the lowest mean MPPE and NRMSE when $n1m1$ and $n1m3$ PV models are used. Their MPPE and NRMSE values can be found in Figs. 11(a) and (b) respectively.

For the SM50 PV module shown in Fig. 11(c), the lowest MPPE and NRMSE occur when using the $n1m2$ and $n2m1$ PV

TABLE IV
SUMMARY OF OPTIMAL PV MODELS USED FOR EACH PV CELL TECHNOLOGY.

PV cell technology	PV model for lowest mean error	
	MPPE	NRMSE
Mono-crystalline	(circuit diagram)	(circuit diagram)
Multi-crystalline	(circuit diagram)	(circuit diagram)
Amorphous silicon	Fig. 2	Fig. 2
Copper indium diselenide	(circuit diagram)	(circuit diagram)
Multi-junction gallium arsenide	(circuit diagram)	(circuit diagram)

models. The lowest MPPE is 0.029 % and the lowest NRMSE is 5.107 %. This illustrates that the MPPE and NRMSE start to increase after the $n2m1$ PV model.

As discussed, the SP70 and UPM250M PV modules have the lowest mean MPPE and mean NRMSE when $n1m1$ and $n1m3$ PV models are used. On the other hand, for the SM50 PV module, the mean MPPE and mean NRMSE are lowest when the $n1m2$ and $n2m1$ PV models are selected.

By comparing the MPPE for SM50 in Fig. 11(c), the difference between the MPPE for $n1m2$ and $n1m1$ PV model is 0.008 %. Hence, we can select the n1m1 PV model for lowest MPPE with some loss of accuracy. Likewise, the difference between the NRMSE for $n2m1$ and $n1m3$ PV model is 0.07 % allowing the $n1m3$ PV model to be used for low NRMSE.

To sum up, the $n1m1$ and $n1m3$ PV models are selected to have low mean MPPE and mean NRMSE for the mono-crystalline PV technology.

For high efficiency MJ-GaAs PV technology, the CTJ30, SLXTJ and ECZTJ PV cells are used. The results show that when $n = 1$ yields the best result. The mean MPPE and NRMSE for the three MJ-GaAs PV cells when $n = 1$ and $m = 1$ to 3 are summarized in Fig. 12.

From Fig. 12, it is observed that the lowest mean MPPE occurs at $n1m2$ with values of 0.253 %, 1.75 % and 1.16 % for the CTJ30, SLXTJ and ECZTJ PV cell respectively. The results also indicate that the mean NRMSE is the lowest at $n1m1$ PV model and it rises with the increase of diodes. From

the results obtained in Fig. 12, the $n1m2$ and $n1m1$ PV models are suitable to achieve low MPPE and NRMSE.
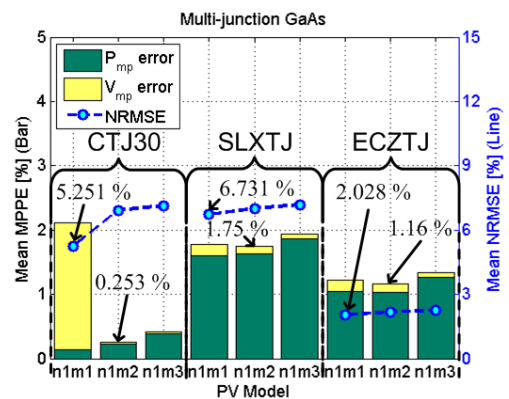
Fig. 12 Mean absolute maximum power point error over T = -25 ℃ to 75 ℃ and mean normalized root mean square error for CTJ30, SLXTJ and ECZTJ multi-junction gallium arsenide PV cell technologies.

Using similar method, the optimal PV models for multi-crystalline, amorphous silicon and CIS are selected. TABLE IV summarizes the optimal PV model for each PV cell technology. From the table, it is observed that the optimal PV models for mono-crystalline and multi-crystalline technology are the same as they are made of similar materials. For both technologies, the $n1m1$ PV model is used for low MPPE showing that they do not require large I-V curve coverage. On the other hand, CIS and MJ-GaAs cell technologies use the

$n1m2$ PV model to achieve low MPPE indicating that larger *I-V* coverage region is required.

Unlike other cell technologies where the optimal PV model is determine by observing the model error, the lowest MPPE and NRMSE occur at different PV model for the amorphous silicon PV modules studied. The lowest mean MPPE and NRMSE obtained for the amorphous PV modules using the proposed method are 0.268 % and 3.567 % respectively. The results are not shown for brevity. Hence, the multi-dimension diode model proposed in this paper can be used to determine the optimal PV models for this cell technology.

VI. CONCLUSION

In this paper, a generalized diode photovoltaic (PV) model is proposed to select optimal model for each PV cell technology. Unlike conventional PV model that only increases the diode in parallel, the proposed PV model allows the diode to be added in series. This leads to an increase in the coverage region of the *I-V* characteristic curve for the PV model. The improved PSO with inverse barrier method is used to identify the parameters of the generalized PV model. Its performance has been benchmarked with the single and double diode PV model. The results show that the proposed method is more accurate.

Based on the lowest mean maximum power point error (MPPE) and normalized root mean square error (NRMSE), the optimal PV models for different cell technologies have been established. They can be used as reference PV model for future works.

REFERENCES

[1] H. L. Tsai, C. S. Tu, and Y. J. Su, "Development of generalized photovoltaic model using MATLAB/SIMULINK," in *Proc. World Congr. Eng. and Comput. Sci.*, 2008.

[2] J. M. Blanes, F. J. Toledo, S. Montero, and A. Garrigos, "In-site real-time photovoltaic I-V curves and maximum power point estimator," *IEEE Trans. Power Electron.*, vol. 28, pp. 1234-1240, Mar. 2013.

[3] K. Ishaque and Z. Salam, "A deterministic particle swarm optimization maximum power point tracker for photovoltaic system under partial shading condition," *IEEE Trans. Ind. Electron.*, vol. 60, pp. 3195-3206, Aug. 2013.

[4] T. L. Nguyen and K. S. Low, "A global maximum power point tracking scheme employing DIRECT search algorithm for photovoltaic systems," *IEEE Trans. Ind. Electron.*, vol. 57, pp. 3456-3467, Oct. 2010.

[5] K. S. Tey and S. Mekhilef, "Modified incremental conductance algorithm for photovoltaic system under partial shading conditions and load variation," *IEEE Trans. Ind. Electron.*, vol. 61, pp. 5384-5392, Oct. 2014.

[6] J. S. C. M. Raj and A. E. Jeyakumar, "A novel maximum power point tracking technique for photovoltaic module based on power plane analysis of I-V characteristics," *IEEE Trans. Ind. Electron.*, vol. 61, pp. 4734-4745, Sep. 2014.

[7] A. N. Celik and N. Acikgoz, "Modelling and experimental verification of the operating current of mono-crystalline photovoltaic modules using four and five-parameter models," *Appli. Energy,* vol. 84, pp. 1-15, Jan. 2007.

[8] M. G. Villalva, J. R. Gazoli, and E. R. Filho, "Comprehensive Approach to Modeling and Simulation of Photovoltaic Arrays," *IEEE Trans. Power Electron.,* vol. 24, pp. 1198-1208, May. 2009.

[9] M. A. G. d. Brito, L. Galotto, L. P. Sampaio, G. d. A. e. Melo, and C. A. Canesin, "Evaluation of the main MPPT techniques for photovoltaic applications," *IEEE Trans. Ind. Electron.,* vol. 60, pp. 1156-1167, Mar. 2013.

[10] R. Kadri, J. P. Gaubert, and G. Champenois, "An improved maximum power point tracking for photovoltaic grid-connected inverter based on voltage-oriented control," *IEEE Trans. Ind. Electron.,* vol. 58, pp. 66-75, Jan. 2011.

[11] B. N. Alajmi, K. H. Ahmed, S. J. Finney, and B. W. Williams, "A maximum power point tracking technique for partially shaded photovoltaic systems in microgrids," *IEEE Trans. Ind. Electron.,* vol. 60, pp. 1596-1606, Apr. 2013.

[12] Y. Mahmoud and E. F. El-Saadany, "A photovoltaic model with reduced computational time," *IEEE Trans. Ind. Electron.,* vol. PP, pp. 1-1, 2014.

[13] J. A. Gow and C. D. Manning, "Development of a photovoltaic array model for use in power-electronics simulation studies," *IEE Proc. Electric Power Applicat.,* vol. 146, pp. 193-200, Mar. 1999.

[14] K. Ishaque, Z. Salam, and H. Taheri, "Simple, fast and accurate two-diode model for photovoltaic modules," *Solar Energy Materials and Solar Cells,* vol. 95, pp. 586-594, Feb. 2011.

[15] L. H. I. Lim, Z. Ye, J. Ye, D. Yang, and H. Du, "A linear identification of diode models from single I-V characteristics of PV panels," *IEEE Trans. Ind. Electron.,* vol. PP, pp. 1-1, 2015.

[16] N. M. A. A. Shannan, N. Z. Yahaya, and B. Singh, "Single-diode model and two-diode model of PV modules: A comparison," in *Proc. IEEE Int. Conf. Control Syst., Computing and Eng. (ICCSCE)*, , Nov. 2013, pp. 210-214.

[17] K. Nishioka, N. Sakitani, Y. Uraoka, and T. Fuyuki, "Analysis of multicrystalline silicon solar cells by modified 3-diode equivalent circuit model taking leakage current through periphery into consideration," *Solar Energy Materials and Solar Cells,* vol. 91, pp. 1222-1227, Aug. 2007.

[18] J. Ma, K. L. Man, T. O. Ting, N. Zhang, S. U. Guan, and W. H. Wong, "Approximate single-diode photovoltaic model for efficient I-V characteristics estimation," *The Scientific World J.,* vol. 2013, p. 7, 2013.

[19] S. Lineykin, M. Averbukh, and A. Kuperman, "Issues in modeling amorphous silicon photovoltaic modules by single-diode equivalent circuit," *IEEE Trans. Ind. Electron.,* vol. 61, pp. 6785-6793, Dec. 2014.

[20] M. S. Ismail, M. Moghavvemi, and T. M. I. Mahlia, "Characterization of PV panel and global optimization of its model parameters using genetic algorithm," *Energy Conversion and Manage.,* vol. 73, pp. 10-25, Sep. 2013.

[21] Y. A. Mahmoud, W. Xiao, and H. H. Zeineldin, "A parameterization approach for enhancing PV model accuracy," *IEEE Trans. Ind. Electron.,* vol. 60, pp. 5708-5716, Dec. 2013.

[22] S. A. Mahmoud, M. M. Alsari, E. I. Reda., and R. M. Alhammadi, "MATLAB modeling and simulation of photovoltaic modules," in *Proc. IEEE 55th Int. Symp. Circuits and Syst.* , Aug. 2012, pp. 786-789.

[23] S. Bal, A. Anurag, and B. C. Babu, "Comparative analysis of mathematical modeling of Photo-Voltaic (PV) array," in *Proc. IEEE Annu. India Conf. (INDICON)*, Dec. 2012, pp. 269-274.

[24] M. Suthar, G. K. Singh, and R. P. Saini, "Comparison of mathematical models of photo-voltaic (PV) module and effect of various parameters on its performance," in *Proc. Int. Conf. Energy Efficient Technologies for Sustainability (ICEETS)*, Apr. 2013, pp. 1354-1359.

[25] J. J. Soon and K. S. Low, "Photovoltaic model identification using particle swarm optimization with inverse barrier constraint," *IEEE Trans. Power Electron.,* vol. 27, pp. 3975-3983, Sep. 2012.

[26] H. Park and H. Kim, "PV cell modeling on single-diode equivalent circuit," in *Proc. IEEE 39th Annu. Conf. Ind. Electron. Soc. (IECON)*, Nov. 2013, pp. 1845-1849.

[27] J. J. Soon and K. S. Low, "Optimizing photovoltaic model parameters for simulation," in *Proc. IEEE Int. Symp. Ind. Electron. Conf. (ISIE)*, May. 2012, pp. 1813-1818.

[28] M. T. Boyd, S. A. Klein, D. T. Reindl, and B. P. Dougherty, "Evaluation and validation of equivalent circuit photovoltaic solar cell performance models," *J. Solar Energy Eng.,* vol. 133, pp. 1-13, May. 2011.

[29] J. J. Soon, K. S. Low, and S. T. Goh, "Multi-dimension diode photovoltaic (PV) model for different PV cell technologies," in *proc. IEEE Int. Symp. Ind. Electron. (ISIE)*, Jun. 2014, pp. 2496-2501.

[30] R. F. Coelho, F. Concer, and D. C. Martins, "A proposed photovoltaic module and array mathematical modeling destined to simulation," in *Proc. IEEE Int. Symp. Ind. Electron, (ISIE)*, Jul. 2009, pp. 1624-1629.

[31] F. Paz and M. Ordonez, "Zero oscillation and irradiance slope tracking for photovoltaic MPPT," *IEEE Trans. Ind. Electron.,* vol. 61, pp. 6138-6147, Nov. 2014.

[32] D. L. King, J. A. Kratochvil, and W. E. Boyson, "Temperature coefficients for PV modules and arrays: measurement methods,

difficulties, and results," in *IEEE 26th Photovoltaic Specialists Conf.*, Sep/Oct.1997, pp. 1183-1186.

[33] W. D. Soto, S. A. Klein, and W. A. Beckman, "Improvement and validation of a model for photovoltaic array performance," *Solar Energy,* vol. 80, pp. 78-88, Jan. 2006.

[34] M. Bashahu and P. Nkundabakura, "Review and tests of methods for the determination of the solar cell junction ideality factors," *Solar Energy,* vol. 81, pp. 856-863, Jul. 2007.

[35] A. J. Bühler and A. Krenzinger, "Method for photovoltaic parameter extraction according to a modified double-diode model," *Progress in Photovoltaics: Research and Applicat.,* vol. 21, pp. 884-893, Mar. 2013.

[36] M. Ye, X. Wang, and Y. Xu, "Parameter extraction of solar cells using particle swarm optimization," *J. Appl. Physics,* vol. 105, pp. 094502-094502-8, May. 2009.

[37] M. Barbato, M. Meneghini, A. Cester, G. Mura, E. Zanoni, and G. Meneghesso, "Influence of shunt resistance on the performance of an illuminated string of solar cells: theory, simulation, and experimental analysis," *IEEE Trans. Device Mater. Rel.,* vol. 14, pp. 942-950, Dec. 2014.

[38] S. Cannizzaro, M. C. D. Piazza, M. Luna, and G. Vitale, "Generalized classification of PV modules by simplified single-diode models," in *Proc. IEEE Int. Symp. Ind. Electron. (ISIE)*, Jun. 2014, pp. 2266-2273.

[39] J. Accarino, G. Petrone, C. A. Ramos-Paja, and G. Spagnuolo, "Symbolic algebra for the calculation of the series and parallel resistances in PV module model," in *Int. Conf. Clean Electric. Power (ICCEP)*, Jun. 2013, pp. 62-66.

[40] G. Segev, G. Mittelman, and A. Kribus, "Equivalent circuit models for triple-junction concentrator solar cells," *Solar Energy Materials and Solar Cells,* vol. 98, pp. 57-65, Mar. 2012.

[41] A. B. Or and J. Appelbaum, "Estimation of multi-junction solar cell parameters," *Progress in Photovoltaics: Research and Applicat.,* vol. 21, pp. 713-723, Jun. 2013.

[42] M. A. d. Blas, J. L. Torres, E. Prieto, and A. García, "Selecting a suitable model for characterizing photovoltaic devices," *Renewable Energy,* vol. 25, pp. 371-380, Mar. 2002.

[43] S. Solar. *SP70 Photovoltaic Solar Module*. Available: http://telemetryhelp.com/Datasheets/ShellSP70_USv1.pdf

[44] S. Solar. *Shell ST40 Photovoltaic Solar Module*. Available: http://telemetryhelp.com/Datasheets/ShellST40_USv1.pdf

[45] KYOCERA. *KD210GH-2PU High Efficiency Multicrystalline Photovoltaic Module*. Available: http://www.kyocerasolar.de/index/products/download/English.-cps-7724-files-8653-File.cpsdownload.tmp/KD210GH-2PU_Eng_January%202009.pdf

[46] R. Lang. (2012). *GSview [Online]*. Available: http://pages.cs.wisc.edu/~ghost/gsview/get50.htm

[47] Upsolar. *UPM250M Monocrystalline PV module 60 cells*. Available: www.upsolar.com/au/products/down.aspx?id=394&type=1

[48] S. Solar. *Shell SM50-H photovoltaic solar module*. Available: www.ecomaipo.cl/solar/documentos/shell-SM50-H.pdf

[49] Upsolar. *UPM280P Polycrystalline PV module 72 cells*. Available: http://www.upsolar.com/eu/products/list.aspx?type=117

[50] S. Solar. *Shell S115 photovoltaic solar module*. Available: www.solarcellsales.com/techinfo/docs/ShellSolarS115_UKv5.pdf

[51] Uni-solar. *Power bond ePVL technical datasheet*. Available: http://www.civicsolar.com/sites/default/files/documents/powerbond20technical20data20sheet-43925.pdf

[52] Marcegaglia. *Flexible photovoltaic laminates MPVL*. Available: www.marcegaglia.com/.../flexibl_photovoltaic_laminates_22_Cells_EN.pdf

[53] W. Solar. *Copper indium diselendide photovolataic modules*. Available: www.jhroerden.com/solar/.../Folleto%20CIS%20WURTH%20inglés.pdf

[54] CESI. *CTJ-30 triple junction solar cell for space applications*. Available: http://www.cesi.it/services/solar_cells/Documents/CTJ30-2015.pdf

[55] Spectrolab. *29.5% NeXt triple junction (XTJ) solar cells*. Available: www.spectrolab.com/DataSheets/.../PV%20XTJ%20Cell%205-20-10.pdf

[56] Emcore. *ZTJ photovoltaic cell, advance triple junction solar cell for space applications*. Available: www.emcore.com/wp-content/uploads/ZTJ-Cell.pdf

Jing Jun Soon (S'12) received the B.Eng. degree in electrical and electronic engineering from Nanyang Technological University, Singapore in 2010. He has submitted his Ph.D thesis in 2014 at the same university.

Currently, he is working at Satellite Research Centre (SaRC), Nanyang Technological University, Singapore as a researcher. During his undergraduate and Ph.D studies, he has been involved in the development of the Power Subsystem for three satellites (VELOX-PII, VELOX-I, VELOX-PIII) which has been launched between November 2013 and June 2014.

His main research interests includes modeling of photovoltaic, maximum power point tracking, power electronics, grid connected power systems and satellite power system. Mr. Soon is the recipient of best conference paper award for IEEE Industrial Electronics and Applications (ICIEA) 2014. He has been a student member of IEEE since 2012.

Kay-Soon Low (M'88-SM'00) received the B.Eng. degree in Electrical Engineering from the National University of Singapore, Singapore, and the Ph.D. degree in Electrical Engineering from the University of New South Wales, Sydney, Australia.

He has worked in the academia as well as in the industry. He joined the School of Electrical and Electronic Engineering, Nanyang Technological University in 1994 first as a lecturer and subsequently became an Associate Professor. He has successfully supervised 42 graduate theses and delivered 43 funded projects. He has served as consultants to many companies and has 19 patents on nonlinear circuits, ultra-wideband radio systems and imaging sensor. His funded projects are in the field of wireless sensor network, power electronics, solar energy and satellite system. He has been the centre director of Satellite Research Centre (SaRC), Nanyang Technological University since April 2009. The centre has successfully developed four satellites (X-SAT, VELOX-PII, VELOX-PIII and VELOX-I) and they have been launched between April 2011 and June 2014. In orbit experiments such as fault tolerant power management system, peak power tracker for solar energy, model predictive control of satellite attitude have been successfully demonstrated.

Dr Low received the IEEE Industrial Electronics and Applications (ICIEA) 2014 best conference paper award, the Singapore Public Administration Medal (Bronze) in 2014, and Defence Technology Prize (Research & Development category) in 2011. He has been a senior member of IEEE since 2000.